Ligand Radicals

DOI: 10.1002/anie.200800669

An Electron-Transfer Series of High-Valent Chromium Complexes with Redox Non-Innocent, Non-Heme Ligands**

Connie C. Lu, Serena DeBeer George, Thomas Weyhermüller, Eckhard Bill, Eberhard Bothe, and Karl Wieghardt**

Dedicated to Professor Bernt Krebs on the occasion of his 70th birthday

Organic radicals that are directly coordinated to a transition metal ion in metalloenzymes can be vital to enzymatic function.[1] An important subfamily of such complexes concerns organic radicals bound to a high-valent metal center. One fascinating example is an iron(IV) oxo species supported by a porphyrin π radical, $[(Porp^{\bullet})Fe{=}O]^{+}$, which has been postulated as an intermediate in the catalytic pathways of cytochromes P450, peroxidases, and catalases.[2] The presence of the porphyrin radical in some of these enzymes and in biomimetic complexes has been confirmed by spectroscopy,[2a,3] however researchers still seek to understand the factors that govern the possible electronic structures (e.g. $[(Porp)Fe^{V}{=}O]^{+}$, $[(Porp^{\bullet})Fe^{IV}{=}O]^{+}$, or $[(Porp)Fe^{IV}{=}O^{\bullet}]^{+}$) and to develop structure–activity relationships.[4]

The coordination chemistry of ligand radicals and high-valent metal centers has also been studied using manganese and chromium oxo complexes with heme-like ligands.[5] However, it is rare among such complexes to find an electron-transfer series wherein the question of metal versus ligand oxidation has been well investigated.[6] Moreover, the structural characterization of these high-valent metal ligand-radical species is often lacking.[7] We now present an electron-transfer series comprising high-valent chromium imide complexes featuring redox-active, non-heme ligands. We were surprised to discover a unique redox event whereupon the addition of two oxidation equivalents ultimately resulted in a more reduced chromium center coordinated to an imidyl radical $(NR^{\bullet})^{-}$. Imidyl metal coordination complexes have yet to be established,[8] and even the coordination chemistry of the related aminyl radical $(NR_2^{\bullet})^{0}$ is limited to only a few examples.[9]

Entry into this work began with the recently reported chromium(II) complex $[(L^{\bullet})_2Cr]$,[10] where $(L^{\bullet})$ represents the monoanionic π radical of the α-iminopyridine ligand 2,6-bis(1-methylethyl)-*N*-(2-pyridinylmethylene)phenylamine (L). Addition of 1-adamantyl azide (AdN_3) to $[(L^{\bullet})_2Cr]$ in benzene at ambient temperature resulted immediately in effervescence of N_2 and a color change from dark brown to royal purple. The solid-state structure revealed the product to be the chromium imido complex $[(L^{\bullet})_2Cr(NAd)]$ [**1**; Eq. (1)].

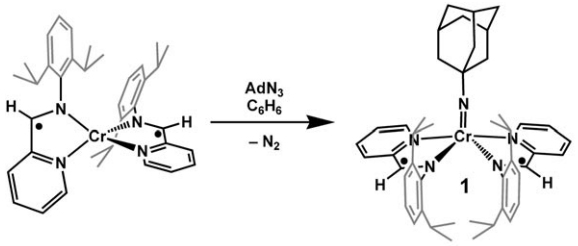

(1)

Compound **1** is diamagnetic ($S=0$), and its cyclic voltammogram (CV) in THF contains a fully reversible redox event at −1.15 V and a quasi-reversible feature at −0.40 V (vs. Fc^{+}/Fc). The reversibility of the latter improves upon increasing the scan rate from 50 to 1000 $mV\,s^{-1}$ (see the Supporting Information). The two features in the CV were assigned as oxidations based on the lack of reactivity of **1** with $[Cp_2Co]$. Conversely, compound **1** reacts readily with one and two equivalents of $[Cp_2Fe][B(3,5\text{-}(CF_3)_2C_6H_3)_4]$ in THF to generate $[(L^{\bullet})(L)Cr(NAd)][B(3,5\text{-}(CF_3)_2C_6H_3)_4]$ (**1**$[B(3,5\text{-}(CF_3)_2C_6H_3)_4]$) and $[(L)_2Cr(NAd)][\{B(3,5\text{-}(CF_3)_2C_6H_3)_4\}_2]$ (**1**$[\{B(3,5\text{-}(CF_3)_2C_6H_3)_4\}_2]$), respectively.

These three compounds together form a one-electron-transfer series $[(L^{x})_2Cr{=}NAd]^{n}$ (for $n=0$–2) wherein the metal and/or ligand(s) are successively oxidized. The effective magnetic moments (μ_{eff}) of $\mathbf{1}^{+}$ and $\mathbf{1}^{2+}$ are virtually temperature-independent from 50 to 290 K at 1.83 and 2.80 μ_B, respectively (see the Supporting Information). These values are close to the expected spin-only values for an $S=1/2$ and an $S=1$ system, respectively. The doublet-spin compound $\mathbf{1}^{+}$ was further characterized by EPR spectroscopy in a THF glass at 10 K. The EPR spectrum shows a nearly isotropic signal with $g=(2.02, 2.00, \text{and } 1.98)$, which unfortunately does not allow

[*] Dr. C. C. Lu, Dr. T. Weyhermüller, Dr. E. Bill, Dr. E. Bothe, Prof. Dr. K. Wieghardt
Max-Planck-Institut für Bioanorganische Chemie
Stiftstrasse 34–36, 45470 Mülheim an der Ruhr (Germany)
Fax: (+49) 208-306-3951
E-mail: ccluck@mpi-muelheim.mpg.de
wieghardt@mpi-muelheim.mpg.de
Dr. S. DeBeer George
Stanford Synchrotron Radiation Laboratory
SLAC, Stanford University
Stanford, CA 94309 (USA)

[**] C.C.L. thanks the Alexander von Humboldt Foundation for a postdoctoral fellowship. SSRL operations are funded by the DOE and BES. The SMB program is supported by the NIH, NCRR, BTP, and by the DOE, BER. This publication was made possible by grant number 5 P41 RR001209 from the NCRR, a component of the NIH. Its contents are the responsibility of the authors and do not represent the official view of the NCRR or NIH.

Supporting information for this article is available on the WWW under http://dx.doi.org/10.1002/anie.200800669.

us to distinguish between a metal- and a ligand-based electron since $g_{Cr} \approx 2.0$ (see the Supporting Information).[11]

The solid-state structures for **1**, $\mathbf{1}^+$, and $\mathbf{1}^{2+}$ are depicted in Figure 1.[12] All structures exhibit a distorted trigonal-bipyramidal geometry wherein the imide and imine nitrogen atoms occupy the equatorial plane (Σ(angles) = 360°), and the two

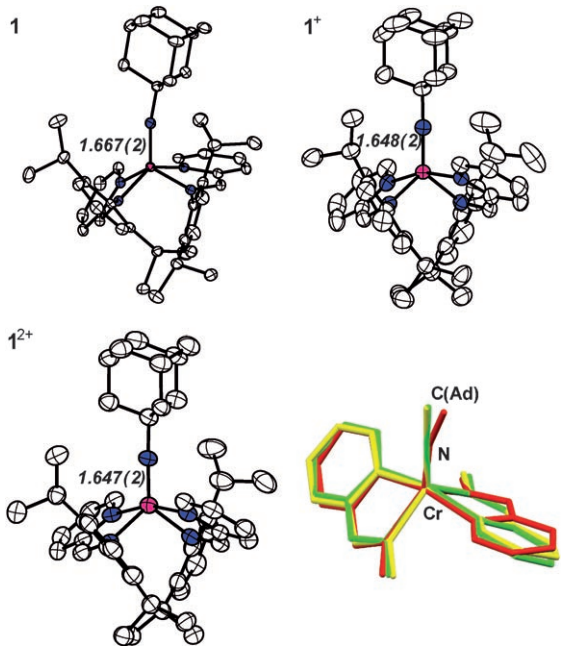

Figure 1. Molecular structures of **1** (top left), $\mathbf{1}^+$ (top right), and $\mathbf{1}^{2+}$ (bottom left; 50% probability level). The counteranion and solvent molecules have been omitted. Bottom right: an overlay of the structural cores of **1** (red), $\mathbf{1}^+$ (yellow), and $\mathbf{1}^{2+}$ (green).

pyridyl nitrogen atoms are nearly axial (162°). An overlay of the structural cores shows that the bond angles around chromium do not vary significantly within the series (Figure 1). The Cr–N(imide) bond distance decreases only slightly from 1.667(2) Å in **1** to 1.648(2) and 1.647(2) Å in $\mathbf{1}^+$ and $\mathbf{1}^{2+}$, respectively. These minute changes in the Cr–N(imide) bond length correlate with the straightening of the Cr–N–C(Ad) bond from 163.6(1)° in **1** to 174.5(2)° and 176.6(3)° in $\mathbf{1}^+$ and $\mathbf{1}^{2+}$, respectively.

Although the gross features in the molecular structures of **1**, $\mathbf{1}^+$, and $\mathbf{1}^{2+}$ are similar, a careful inspection of the α-iminopyridine ligand bond parameters does reveal significant differences (Table 1). Thus, the bond lengths in the ligand backbone vary by up to 0.07 Å, which reflects a redox-state change in the ligand of one electron (Scheme 1). A comparison of the backbone bond lengths for **1** and $\mathbf{1}^{2+}$ shows that both ligands are consistent with the monoanionic π* radical form in **1** and the neutral α-iminopyridine in $\mathbf{1}^{2+}$.[10] The bond lengths of the two ligands in the monocation $\mathbf{1}^+$ lie between those expected for the closed-shell neutral ligand and for the monoanionic π radical, thereby making it less straightforward to assign oxidation states. The two ligands in $\mathbf{1}^+$ do appear inequivalent, however, with one of the ligand parameters approaching the radical state and the other the neutral form.

Table 1: Experimental bond lengths [Å] in the ligand backbone.

bond[a]	**1**	$\mathbf{1}^+$	$\mathbf{1}^{2+}$
C–C	1.396(3)	1.408(4)	1.458(6)
C–N(iminyl)	1.351(2)	1.328(3)	1.284(5)
C–N(pyridyl)	1.384(2)	1.365(3)	1.370(5)
C–C	1.402(2)	1.435(4)	1.466(6)
C–N(iminyl)	1.337(2)	1.299(3)	1.281(5)
C–N(pyridyl)	1.387(2)	1.364(3)	1.377(5)

[a] The distances for each ligand are presented separately.

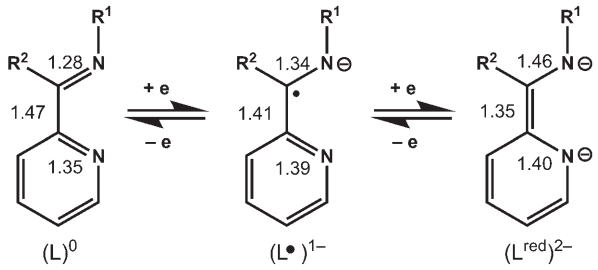

Scheme 1. Characteristic bond lengths in the different ligand redox states. The bond parameters for $(L^{\bullet})^-$ and $(L^{red})^{2-}$ are based on a small number of complexes and should be used cautiously.

This suggests the presence of one ligand radical in $\mathbf{1}^+$. Based on the solid-state structures, the redox changes in this electron-transfer series are likely to be occurring at the ligand sites. As a consequence, the redox state of the $(CrNAd)^{2+}$ fragment appears unaltered in the series.

The presence of ligand radical(s) in **1** and $\mathbf{1}^+$ is also evident by their intense colors relative to $\mathbf{1}^{2+}$, where both ligands are in their closed-shell neutral form. The electronic absorption spectra for the series are shown in Figure 2. Compounds **1** and $\mathbf{1}^+$ are characterized by absorptions with large extinction coefficients (approx. $10^4\ M^{-1}cm^{-1}$) in the UV/Vis and NIR regions, whereas the dication $\mathbf{1}^{2+}$ has no strong absorptions ($\varepsilon \leq 1\ M^{-1}cm^{-1}$). An intervalence charge-transfer band is observed for $\mathbf{1}^+$ at 1310 nm.

X-ray absorption spectroscopy (XAS) studies were conducted to investigate the oxidation state of the chromium center as the pre-edge region can be a particularly sensitive probe of the local metal electronic structure.[13,14] Figure 3 displays the Cr K-edge data for **1**, $\mathbf{1}^+$, and $\mathbf{1}^{2+}$. The pre-edge

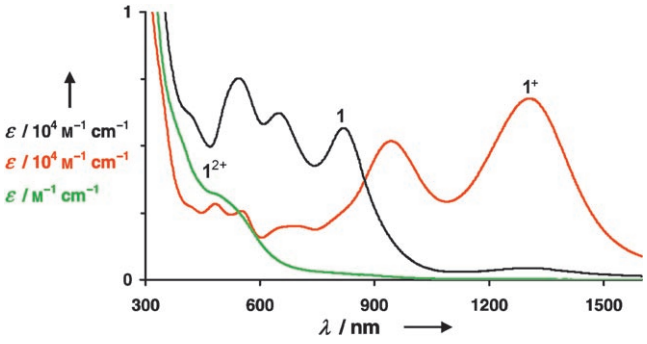

Figure 2. Electronic absorption spectra of **1**, $\mathbf{1}^+$, and $\mathbf{1}^{2+}$ in THF at 22 °C.

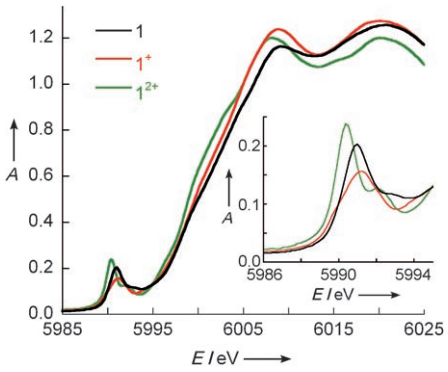

Figure 3. Comparison of the normalized Cr K-edge XAS spectra for **1**, $\mathbf{1}^{+}$, and $\mathbf{1}^{2+}$. The inset shows a close-up of the pre-edge features.

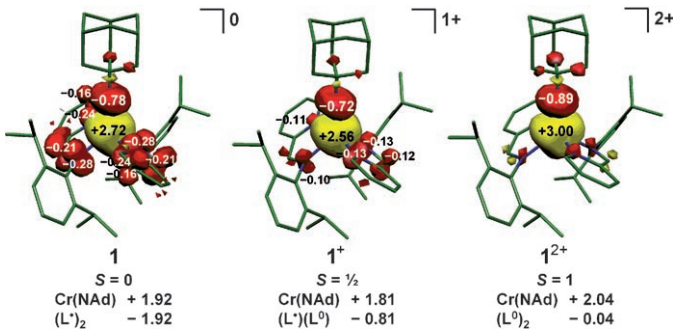

Figure 4. Spin-density distribution and values for the hybrid DFT models of **1** BS(2,2), $\mathbf{1}^{+}$ BS(2,1), and $\mathbf{1}^{2+}$. Only atoms with spin densities ≥ 0.10 are labeled.

(5990.7 (**1**) and 5990.9 eV ($\mathbf{1}^{+}$)) and rising-edge shifts for **1** and $\mathbf{1}^{+}$ are consistent with Cr^{IV}.[14] A tetravalent chromium center also correlates with the observed diamagnetism of **1** and the doublet state of $\mathbf{1}^{+}$ by the following rationale. If ligand radical(s) are present, then the spin of the ligand radical(s) ($S_{Lig} = {}^{1}/_{2}$) may couple antiferromagnetically to the metal spin (Cr^{IV}, $S_{Cr} = 1$). In the case of **1**, the two ligand radicals effectively cancel the metal spin to give a singlet state, whereas in $\mathbf{1}^{+}$ the sole ligand radical couples to Cr^{IV} to generate a doublet state. Another outcome of a tetravalent metal state is that the imide group must be the closed-shell dianion $(NAd)^{2-}$, which is the expected oxidation state for this functionality. In contrast to **1** and $\mathbf{1}^{+}$, the dication $\mathbf{1}^{2+}$ has energetically lower pre-edge (5990.1 eV) and rising-edge (by about 1 eV) positions, which are indicative of a reduced Cr^{III} center.[15] This finding is surprising because we would have to invoke an anionic imidyl radical $(NAd)^{\bullet-}$ rather than the typical closed-shell dianion $(NAd)^{2-}$ to account for a Cr^{III} state in $\mathbf{1}^{2+}$.[16]

To further elucidate the electronic structures, broken-symmetry (BS) hybrid density functional theory (DFT) calculations were conducted (B3LYP). The calculated geometries were generally in good agreement with the experimental ones (see the Supporting Information). The spin-density maps for the theoretical models of **1**, $\mathbf{1}^{+}$, and $\mathbf{1}^{2+}$ are shown in Figure 4. The number of unpaired electrons on the ligands is two, one, and zero for **1**, $\mathbf{1}^{+}$, and $\mathbf{1}^{2+}$ respectively. The net spin density for the $(CrNAd)^{2+}$ unit in all models is around 2, although the spin density at chromium, which varies from 2.6 to 3.0, reflects a continuum between Cr^{IV} and Cr^{III}.

The molecular orbital (MO) diagram for $\mathbf{1}^{2+}$ is shown in Figure 5. Five predominantly metal-based MOs, two of which are singly occupied, are found. Notably, the next two high-lying MOs (which correspond to the anti-bonding π* interaction between Cr and NAd) contain significant covalent contributions from the imido nitrogen atom, therefore the occupation of their congeners (the π-bonding interaction between Cr and NAd, which is presumably at lower energy) raises the spin density at Cr above two and towards three. The d orbitals of **1** and $\mathbf{1}^{+}$ are also doubly occupied, with the only significant differences occurring at the ligands. The ligand π* orbital(s) in **1** and $\mathbf{1}^{+}$ become singly occupied and their electron(s) magnetically couple to the d electrons(s) of

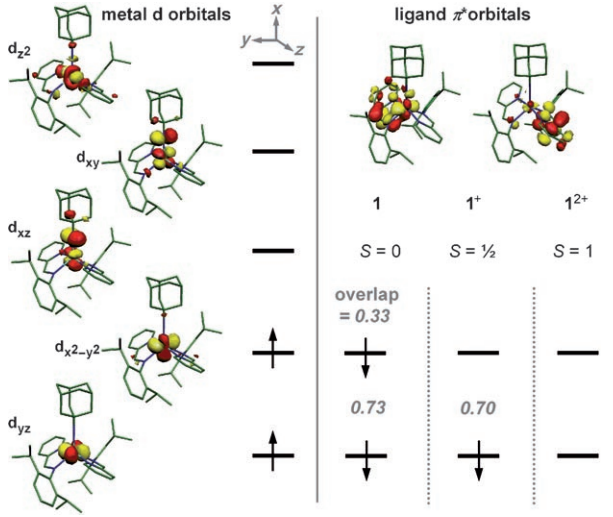

Figure 5. Qualitative MO diagrams of the magnetic orbitals derived from the hybrid DFT calculations of **1** BS(2,2), $\mathbf{1}^{+}$ BS(2,1), and $\mathbf{1}^{2+}$. The spatial overlaps of the corresponding alpha and beta orbitals are given.

chromium. The DFT calculations clearly show the presence or absence of radical(s) in the iminopyridine ligands. Disappointingly, however, the calculations do not exactly reproduce the observed dramatic change in the chromium oxidation state, although they do suggest that two different extremes of electronic structures are possible for the $(CrNAd)^{2+}$ unit—$(Cr^{IV}(NAd)^{2-})^{2+}$ or $(Cr^{III}(NAd)^{\bullet-})^{2+}$. According to Cr K-edge data, the former is valid for **1** and $\mathbf{1}^{+}$ whereas the latter is a more fitting descriptor for $\mathbf{1}^{2+}$.

In summary, an electron-transfer series featuring high-valent chromium and ligand-centered radicals has been described for non-heme ligands. The electronic structures shown in Equation (2) can be proposed for this series based on structural/spectroscopic evidence in conjunction with DFT calculations. We observe the counter-intuitive correlation that the metal oxidation state decreases as the overall oxidation level increases ($\mathbf{1} \rightarrow \mathbf{1}^{+} \rightarrow \mathbf{1}^{2+}$). One explanation for this is that

$$[(L^{\bullet})_2Cr^{IV}{=}\ddot{N}Ad]^{0} \underset{+e}{\overset{-e}{\rightleftharpoons}} [(L^{\bullet})(L)Cr^{IV}{=}\ddot{N}Ad]^{1+} \underset{+e}{\overset{-e}{\rightleftharpoons}} [(L)_2Cr^{III}{=}\dot{N}Ad]^{2+} \quad (2)$$

$\mathbf{1}$ $\quad\quad$ $\mathbf{1}^{+}$ $\quad\quad$ $\mathbf{1}^{2+}$

removal of the ligand radicals may increase the π-backbonding interactions between Cr and the α-iminopyridines. The electron density lost by the metal through π-backbonding may be compensated from the π-donating imido group. Consequently, the stability of the imide $(NAd)^{2-}$ anion against oxidation decreases with increasing oxidation levels until the imidyl radical $(NAd)^{\bullet-}$ is ultimately stabilized, with concomitant reduction of the metal from a formal Cr^{IV} ion in **1** and $\mathbf{1}^{+}$ to Cr^{III} in $\mathbf{1}^{2+}$. In conclusion, the complexity of accessible electronic configurations is underscored not only by the redox non-innocence of the α-iminopyridine ligands and the imido functionality, but also by the intricate interplay between their oxidation states and that of the metal center.

Experimental Section

All syntheses were carried out inside a glovebox under argon at ambient temperature. See the Supporting Information for details regarding physical methods.

1: 1-Adamantyl azide (70.9 mg, 388 μmol) was added to a solution of $[(L^{\bullet})_2Cr]$ (226.9 mg, 388 μmol) in benzene (10 mL). The solution immediately effervesced and changed color from dark brown to a dark royal purple. After stirring for 2 h, the solvent was removed under vacuum and the resulting crude residue was washed liberally with pentane. Yield: 206 mg (72%). Single crystals were grown from a diethyl ether solution by slow evaporation. ^{1}H NMR (400 MHz, C_6D_6, 22 °C): $\delta = 7.56$ (d, $J_{H,H} = 6.1$ Hz, 1H), 7.21 (m, 2H), 7.10 (d, $J_{H,H} = 7.5$ Hz, 1H), 6.70 (d, $J_{H,H} = 8.5$ Hz, 1H), 6.16 (app t, $J_{H,H} = 7$ Hz, 2H), 4.98 (br, 1H), 3.36 (sept, $J_{H,H} = 6.6$ Hz, 1H; C*H*(Me)$_2$), 2.45 (sept, $J_{H,H} = 6.6$ Hz, 1H; C*H*(Me)$_2$), 1.93 (br, 3H; Ad), 1.86 (br, 6H; Ad), 1.49 (app q, $J_{H,H} = 12.5$ Hz, 6H; Ad), 1.36 (d, $J_{H,H} = 6.5$ Hz, 6H; CH*Me*Me), 1.19 (d, $J_{H,H} = 6.5$ Hz, 6H; CH*Me*Me), 1.05 (d, $J_{H,H} = 6.5$ Hz, 6H; CH*Me*Me), 0.99 ppm (d, $J_{H,H} = 6.5$ Hz, 6H; CH*Me*Me); ^{13}C NMR (400 MHz, C_6D_6, 22 °C): $\delta = 149.8, 148.5, 145.1, 144.9, 144.4, 126.8, 126.2, 124.6, 123.4, 123.2, 45.4, 36.6, 29.9, 28.2, 27.7, 27.0, 26.9, 24.1, 22.0$ ppm; UV/Vis/NIR (THF): λ_{max} (ε) = 820 (5660), 650 (6210), 540 nm (7520) $10^3\,M^{-1}\,cm^{-1}$; elemental analysis (%) calcd for $C_{46}H_{59}CrN_5$: C 75.27, H 8.10, N 9.54; found: C 75.11, H 8.15, N 9.39.

$\mathbf{1}^{+}$: One equivalent of $[Cp_2Fe][B(3,5\text{-}(CF_3)_2C_6H_3)_4]$ (195.0 mg, 186 μmol) was added to a solution of **1** (136.4 mg, 185.8 μmol) in THF (10 mL). After stirring for 8 h, the solvent was removed under vacuum and the resulting residue washed liberally with hexane. Crystals of $\mathbf{1}[B(3,5\text{-}(CF_3)_2C_6H_3)_4]$ were grown by vapor diffusion of pentane into a concentrated THF solution (217 mg, 73% yield). UV/Vis/NIR (THF): λ_{max} (ε) = 1310 (6770), 940 (5170), 680 (2000), 550 (2570), 480 nm (2830) $10^3\,M^{-1}\,cm^{-1}$; elemental analysis (%) calcd for $C_{78}H_{71}BCrF_{24}N_5$: C 58.65, H 4.48, N 4.38; found: C 59.02, H 4.42, N 4.06.

$\mathbf{1}^{2+}$: Two equivalents of $[Cp_2Fe][B(3,5\text{-}(CF_3)_2C_6H_3)_4]$ (195.0 mg, 186 μmol) were added to a solution of **1** (127.1 mg, 173.2 μmol) in THF (10 mL). After stirring for 8 h, the solvent was removed under vacuum and the resulting residue washed liberally with hexane. Yield: 410 mg (95%). Single crystals of $\mathbf{1}[\{B(3,5\text{-}(CF_3)_2C_6H_3)_4\}]_2]$ were grown from a CH_2Cl_2 solution by slow evaporation; elemental analysis (%) calcd for $C_{110}H_{83}B_2CrF_{48}N_5$: C 53.70, H 3.40, N 2.85; found: C 53.42, H 3.49, N 2.74.

Received: February 11, 2008
Revised: May 13, 2008
Published online: July 11, 2008

Keywords: bioinorganic chemistry · chromium · electron transfer · N ligands · radicals

[1] a) J. Stubbe, W. A. van der Donk, *Chem. Rev.* **1998**, *98*, 705–762; b) M. Sono, M. P. Roach, E. D. Coulter, J. H. Dawson, *Chem. Rev.* **1996**, *96*, 2841–2888.

[2] a) *Handbook of Metalloproteins*, *Vol. 1* (Eds.: A. Messerschmidt, R. Huber, T. Poulos, K. Wieghardt), Wiley, Chichester, **2001**, pp. 193–328; b) T. L. Poulos in *The Porphyrin Handbook*, *Vol. 4* (Eds: K. M. Kadish, K. M. Smith, R. Guilard), Academic Press, San Diego, **2000**, pp. 189–218.

[3] a) H. Fujii, *Coord. Chem. Rev.* **2002**, *226*, 51–60; b) J. T. Groves, R. C. Haushalter, M. Nakamura, T. E. Nemo, B. J. Evans, *J. Am. Chem. Soc.* **1981**, *103*, 2884–2886.

[4] a) J. H. Dawson, *Science* **1988**, *240*, 433–439; b) D. L. Harris, *Curr. Opin. Chem. Biol.* **2001**, *5*, 724–735; c) R. Weiss, V. Bulach, A. Gold, J. Terner, A. X. Trautwein, *J. Biol. Inorg. Chem.* **2001**, *6*, 831–845; d) A. Ghosh, E. Steene, *J. Biol. Inorg. Chem.* **2001**, *6*, 739–752.

[5] a) W. J. Song, M. S. Seo, S. DeBeer George, T. Ohta, R. Song, M.-J. Kang, T. Tosha, T. Kitagawa, E. I. Solomon, W. Nam, *J. Am. Chem. Soc.* **2007**, *129*, 1268–1277, and references therein; b) Z. Gross, *J. Biol. Inorg. Chem.* **2001**, *6*, 733–738; c) R. D. Arasasingham, T. C. Bruice, *Inorg. Chem.* **1990**, *29*, 1422–1427; d) S. H. L. Wang, B. S. Mandimutsira, R. Todd, B. Ramdhanie, J. P. Fox, D. P. Goldberg, *J. Am. Chem. Soc.* **2004**, *126*, 18–19.

[6] A. E. Meier-Callahan, A. J. Di Bilio, L. Simkhovich, A. Mahammed, I. Goldberg, H. B. Gray, Z. Gross, *Inorg. Chem.* **2001**, *40*, 6788–6793.

[7] This is also the case for high-valent Cr and Mn imide complexes with redox-non-innocent heme-like ligands: a) N. Y. Edwards, R. A. Eikey, M. I. Loring, M. M. Abu-Omar, *Inorg. Chem.* **2005**, *44*, 3700–3708; b) B. Moubaraki, K. S. Murray, P. J. Nichols, S. Thomson, B. O. West, *Polyhedron* **1994**, *13*, 485–495.

[8] E. Kogut, H. L. Wiencko, L. Zhang, D. E. Cordeau, T. H. Warren, *J. Am. Chem. Soc.* **2005**, *127*, 11248–11249.

[9] a) T. Büttner, J. Geier, G. Frison, J. Harmer, C. Calle, A. Schweiger, H. Schönberg, H. Grützmacher, *Science* **2005**, *307*, 235–238; b) F. N. Penkert, T. Weyhermüller, E. Bill, P. Hildebrandt, S. Lecomte, K. Wieghardt, *J. Am. Chem. Soc.* **2000**, *122*, 9663–9673.

[10] C. C. Lu, E. Bill, T. Weyhermüller, E. Bothe, K. Wieghardt, *J. Am. Chem. Soc.* **2008**, *130*, 3181–3197.

[11] J.-J. Girerd, Y. Journaux in *Physical Methods in Bioinorganic Chemistry* (Ed.: L. Que, Jr.), University Science Books, Sausalito, **2000**, pp. 321–373.

[12] CCDC 669778 (**1**), CCDC 669779 ($\mathbf{1}^{+}$), and CCDC 669780 ($\mathbf{1}^{2+}$) contain the supplementary crystallographic data for this paper. These data can be obtained free of charge from The Cambridge Crystallographic Data Centre via www.ccdc.cam.ac.uk/data_request/cif.

[13] a) T. E. Westre, P. Kennepohl, J. G. DeWitt, B. Hedman, K. O. Hodgson, E. I. Solomon, *J. Am. Chem. Soc.* **1997**, *119*, 6297–6314; b) J. L. DuBois, P. Mukherjee, T. D. P. Stack, B. Hedman, E. I. Solomon, K. O. Hodgson, *J. Am. Chem. Soc.* **2000**, *122*, 5775–5787.

[14] a) R. Kapre, K. Ray, I. Sylvestre, T. Weyhermüller, S. DeBeer George, F. Neese, K. Wieghardt, *Inorg. Chem.* **2006**, *45*, 3499–3509; b) R. R. Kapre, E. Bothe, T. Weyhermüller, S. DeBeer George, N. Muresan, K. Wieghardt, *Inorg. Chem.* **2007**, *46*, 7827–7839.

[15] Observed shifts in the pre-edge peak typically correspond to approximately 1 eV per oxidation state for first-row metals.

[16] DFT calculations of strong, covalent metal–X bonds (where X = O, N) have been reported to exhibit spin densities wherein a full unpaired electron resides on X. For examples, see: a) A. Decker, E. I. Solomon, *Angew. Chem.* **2005**, *117*, 2292–2295; *Angew. Chem. Int. Ed.* **2005**, *44*, 2252–2255; b) N. Aliaga-Alcalde, S. DeBeer George, B. Mienert, E. Bill, K. Wieghardt, F. Neese, *Angew. Chem.* **2005**, *117*, 2968–2972; *Angew. Chem. Int. Ed.* **2005**, *44*, 2908–2912.

